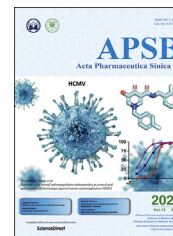




Chinese Pharmaceutical Association  
Institute of Materia Medica, Chinese Academy of Medical Sciences

Acta Pharmaceutica Sinica B

[www.elsevier.com/locate/apsb](http://www.elsevier.com/locate/apsb)  
[www.sciencedirect.com](http://www.sciencedirect.com)



ORIGINAL ARTICLE

# Multiparametric characterization of red blood cell physiology after hypotonic dialysis based drug encapsulation process



Mélanie Robert<sup>a,b,c</sup>, Bastien Laperrousaz<sup>a</sup>, Diana Piedrahita<sup>a</sup>,  
Emilie-Fleur Gautier<sup>c,d</sup>, Travis Nemkov<sup>e,f</sup>, Florian Dupuy<sup>c,g</sup>,  
Elie Nader<sup>b,c</sup>, Virginie Salnot<sup>d</sup>, Patrick Mayeux<sup>c,d</sup>,  
Angelo D'Alessandro<sup>e,f</sup>, Catherine Lavazec<sup>c,g</sup>, Philippe Joly<sup>b,c,h</sup>,  
Alexander Scheer<sup>a</sup>, Philippe Connes<sup>b,c,#</sup>, Agnès Cibiel<sup>a,#,\*</sup>

<sup>a</sup>Erytech Pharma, Lyon 69008, France

<sup>b</sup>Laboratoire interuniversitaire de Biologie de la Motricité (LIBM) EA7424, Team « Vascular Biology and Red Blood Cell », Université Claude Bernard Lyon 1, Université de Lyon, Lyon 69008, France

<sup>c</sup>Labex GR-Ex, Paris 75015, France

<sup>d</sup>3P5 proteom'IC facility, Université de Paris, Institut Cochin, INSERM, CNRS, Paris 75014, France

<sup>e</sup>University of Colorado, Anschutz Medical Campus, Aurora, CO 80045, USA

<sup>f</sup>Omix Technologies, Inc., Aurora, CO 80045, USA

<sup>g</sup>Inserm U1016, CNRS 8104, Université de Paris, Institut Cochin, Paris 75014, France

<sup>h</sup>Laboratoire de Biochimie et de Biologie Moléculaire, UF de biochimie des pathologies érythrocytaires, Centre de Biologie et de Pathologie Est, Hospices Civils de Lyon, Bron 69500, France

Received 13 July 2021; received in revised form 21 September 2021; accepted 12 October 2021

## KEY WORDS

Red blood cells;  
Drug carrier;  
Hypotonic dialysis;  
L-Asparaginase;  
Omics;  
Rheology;

**Abstract** Red blood cells (RBCs) can act as carriers for therapeutic agents and can substantially improve the safety, pharmacokinetics, and pharmacodynamics of many drugs. Maintaining RBCs integrity and lifespan is important for the efficacy of RBCs as drug carrier. We investigated the impact of drug encapsulation by hypotonic dialysis on RBCs physiology and integrity. Several parameters were compared between processed RBCs loaded with L-asparaginase (“eryaspase”), processed RBCs without drug and non-processed RBCs. Processed RBCs were less hydrated and displayed a reduction of intracellular content. We observed a change in the metabolomic but not in the proteomic profile of processed

\*Corresponding author.

E-mail address: [agnes.cibiel@erytech.com](mailto:agnes.cibiel@erytech.com) (Agnès Cibiel).

#Co-last authors.

Peer review under responsibility of Chinese Pharmaceutical Association and Institute of Materia Medica, Chinese Academy of Medical Sciences.

<https://doi.org/10.1016/j.apsb.2021.10.018>

2211-3835 © 2022 Chinese Pharmaceutical Association and Institute of Materia Medica, Chinese Academy of Medical Sciences. Production and hosting by Elsevier B.V. This is an open access article under the CC BY-NC-ND license (<http://creativecommons.org/licenses/by-nc-nd/4.0/>).

Morphology;  
Senescence markers

RBCs. Encapsulation process caused moderate morphological changes and was accompanied by an increase of RBCs-derived Extracellular Vesicles release. Despite a decrease in deformability, processed RBCs were not mechanically retained in a spleen-mimicking device and had increased surface-to-volume ratio and osmotic resistance. Processed RBCs half-life was not significantly affected in a mouse model and our previous phase 1 clinical study showed that encapsulation of asparaginase in RBCs prolonged its *in vivo* half-life compared to free forms. Our study demonstrated that encapsulation by hypotonic dialysis may affect certain characteristics of RBCs but does not significantly affect the *in vivo* longevity of RBCs or their drug carrier function.

© 2022 Chinese Pharmaceutical Association and Institute of Materia Medica, Chinese Academy of Medical Sciences. Production and hosting by Elsevier B.V. This is an open access article under the CC BY-NC-ND license (<http://creativecommons.org/licenses/by-nc-nd/4.0/>).

## 1. Introduction

The development of drug encapsulation systems is gaining increasing attention as a mean to improve safety and efficacy over conventional drug administration systems. As such, red blood cells (RBCs) represent an attractive and valuable opportunity to serve as carriers of encapsulated therapeutic agents. RBCs display many advantages as drug carriers such as biocompatibility, long circulating lifespan and an established sourcing in blood banks. Their membrane shielding properties reduce the toxicity and extend the half-life of entrapped compounds, making them good candidates for *in vivo* drug delivery<sup>1–3</sup>. Many systems of drug encapsulation have been described, such as cell penetrating peptide<sup>4</sup>, electroporation<sup>5,6</sup> or shear-induced encapsulation<sup>7</sup>. However, the most common technique remains osmotic-shock<sup>8</sup>. Briefly, RBCs are placed in hypotonic medium to promote swelling and the formation of pores, allowing the passive entry of therapeutic compounds inside RBCs. Finally, hypertonic medium is added to reseal the pores and entrap compounds inside RBCs. However, RBCs swelling and shrinking during osmotic encapsulation could alter some of their properties and shorten their lifespan, limiting the half-life of the encapsulated drug. Thus, it is essential to assess the integrity of RBCs after encapsulation process to ensure they can achieve their function of drug carriers. Depending on the osmotic-encapsulation process used, several parameters (mean corpuscular volume and hemoglobin, osmotic fragility, morphology, and phosphatidylserine exposure) have been described as being modulated more or less<sup>9–15</sup>.

ERYCAPS® is an industrialized, automated encapsulation process based on hypotonic dialysis principle. Eryaspase, L-asparaginase (ASNase) entrapped inside RBCs, acts as a circulating bioreactor, actively transporting plasmatic asparagine and glutamine into erythrocytes where they are hydrolyzed into aspartate, glutamate and ammonia, respectively. Eryaspase demonstrated promising activity, with a prolonged enzyme activity and reduced allergic reactions compared to the free-form ASNase in acute lymphoblastic leukemia<sup>16</sup>, as well as an improved overall survival in patients with relapsed pancreatic adenocarcinoma<sup>17</sup>. Eryaspase is currently undergoing further investigation in a pivotal phase 3 study, trybeca-1 (NCT03665441) in pancreatic cancer and in a phase 2 study, trybeca-2 (NCT03674242) in triple negative breast cancer.

The aim of this study was to evaluate the impact of hypotonic dialysis using ERYCAPS® encapsulation process on RBCs physiology and integrity, to ensure they can properly achieve their function as drug carriers. For this purpose, a multiparametric analysis was performed focusing on key parameters reflecting RBCs physiology and their aging state. Hematological parameters,

RBCs morphology, proteomic and metabolomic profiles, RBCs deformability and retention rate through a microbead system mimicking the mechanical sensing of spleen, lesion markers such as PS, CD47 content, number of RBCs-derived Extracellular Vesicles released, as well as *in vivo* biodistribution in a mouse model, were assessed after encapsulation process with and without ANSase encapsulation and compared to non-processed RBCs.

## 2. Material and methods

### 2.1. ERYCAPS® encapsulation process and sample preparation

Eryaspase batches were prepared as follows. ASNase (Spectrila®, Medac) was loaded inside RBCs using ERYCAPS® device based on hypotonic dialysis principle. Human leukoreduced packed RBCs stored for less than 10 days were obtained from French blood bank and were used as starting material. RBCs were washed four times with 0.9% NaCl solution and were concentrated to 80% hematocrit (Hct). ASNase was added and RBCs suspension was introduced into a dialyzer at room temperature with hypotonic solution allowing the loading of ASNase into RBCs. Hypertonic solution then was added to reseal RBCs and revert to isotonic conditions. RBCs suspension was incubated 30 min at 37 °C and washed four times with 0.9% NaCl, 0.2% glucose solution. The concentration of ASNase was between 75 and 160 U/mL in the final product. Processed RBCs without ASNase encapsulated (proRBCs) were also prepared following the same procedure. All the final products (proRBCs and eryaspase) and their corresponding non-processed packed RBCs (pRBCs) were adjusted to 45% Hct in AS3 preservative solution and stored at 4 °C until analysis. In proteomic and metabolomic analysis, proRBCs and eryaspase were produced from the same bag of non-processed packed RBCs (pRBCs) to prevent donor variability while for the other parameters proRBCs and eryaspase were produced from different pRBCs bags. Proteomic and metabolomic analysis were performed on samples collected the day of manufacturing, while the other parameters were analyzed one day after.

### 2.2. Hematological parameters

Hematological parameters were measured using a hematological analyzer (Excell 2280, Drew Scientific). Free hemoglobin (Hb) concentration was measured in RBCs supernatant after centrifugation at 1000×g for 10 (min) at room temperature (RT). Hemolysis percentage was calculated as in Eq. (1):

$$\text{Hemolysis percentage (\%)} = (100 - \text{Hct}) \times \text{Free Hb} / \text{Total Hb} \quad (1)$$

### 2.3. Proteomic analysis

Total and ghost RBCs were prepared for proteomic analysis. Ghost RBCs are RBCs with removed intracellular content allowing the detection of low copy number membrane proteins. Prior to proteomic analysis, the purity of RBCs samples was controlled by assessing reticulocyte, leukocyte and platelet content. Leukocytes and platelets levels were measured using a hematological analyzer (Excell 2280, Drew Scientific, Miami Lakes, FL, USA), and reticulocytes were quantified by flow-cytometry (MACSQuant Analyzer 10, Miltenyi, Bergisch Gladbach, Germany) after Retic-count reagent staining (BD Bioscience, San Jose, CA, USA). Low levels of platelets, leukocytes (under detection threshold; *i.e.*,  $<5$  and  $1 \cdot 10^3$  cells/ $\mu\text{L}$ , respectively) and reticulocytes ( $<0.6\%$ ) were observed. RBCs samples were then centrifuged at  $200 \times g$  for 15 min at  $4^\circ\text{C}$ . Supernatant was discarded and RBCs were washed twice in  $1 \times \text{PBS}$ .  $5 \mu\text{L}$  of RBCs pellet was frozen at  $-80^\circ\text{C}$  for total RBCs analysis. The remaining part ( $500 \mu\text{L}$ ) was resuspended in lysis buffer ( $5 \text{ mmol/L Na}_2\text{HPO}_4$ ,  $0.3 \text{ mmol/L EDTA}$ , pH 8; two volume of lysis buffer for one volume of RBCs) and incubated for 20 min at  $4^\circ\text{C}$ . RBCs membranes were pelleted by centrifugation at  $21,500 \times g$  for 15 min and at  $4^\circ\text{C}$ . Supernatant was discarded and sequential washes of ghost pellet were performed in lysis buffer until a white pellet (ghost RBCs) was obtained. Ghosts were frozen at  $-80^\circ\text{C}$  pending analysis. Total and ghost RBCs were digested by filter-assisted sample preparation (FASP) using trypsin. Resulting peptides were fractionated on strong cation exchange chromatography (SCX) StageTips in five different fractions. Peptides from each of these five fractions were separated by C18 rapid separation liquid chromatography (RSLC) Dionex U3000 on a  $2 \mu\text{m}$  particle size,  $100 \text{ \AA}$  pore size,  $75 \mu\text{m}$  internal diameter,  $25 \text{ cm}$  length C18 reverse phase analytical column with a 3 h binary gradient from 99% solution A (0.1% formic acid in  $\text{H}_2\text{O}$ ) to 55% solution B (80% ACN, 0.085% formic acid) before injection into an Orbitrap Fusion mass spectrometer (from Thermo Scientific). The Orbitrap Fusion mass spectrometer acquired data throughout the elution process and operated in a data-dependent scheme (top speed mode in 3 s) with full mass spectrometry (MS) scans acquired with the orbitrap detector, followed by HCD fragmentation and Ion trap fragment detection of the most abundant ions detected in the MS scan. Mass spectrometer settings for full scan MS were:  $1.0\text{E}6$  AGC,  $60,000$  target resolution,  $350\text{--}1500 m/z$  range, maximum injection time of 60 ms. HCD MS/MS fragmentation was permitted for 2–7+ precursor ions reaching more than  $5.0\text{E}4$  minimum intensity. Quadrupole-filtered precursors within  $1.6 m/z$  isolation window were fragmented with a 30 Normalised Collision Energy setting.  $1.0\text{E}5$  AGC Target and 60 ms maximum injection time were the limiting ions accumulation values. The Ion-trap detector was used for its fast and sensitive detection capabilities. A 30 s dynamic exclusion time was set. Maxquant software version 1.6.2.6 was used for the analysis of raw data from mass spectrometer. The following thresholds were used for protein identification: PSM FDR: 0.01, Protein FDR: 0.01, Minimum peptide length: 7, Minimum razor peptides: 1, Minimum peptides: 1, Label minimum ratio count for the calculation of an LFQ intensity: 2. Perseus version 1.6.1.1 and Excel softwares were used for data formatting and statistical analysis. Absolute protein quantification was performed as previously described<sup>18</sup>. Briefly, mean corpuscular hemoglobin (MCH) was used as internal standard for protein quantification in total RBCs samples. Quantification of ankyrin 1

protein was performed in total RBCs samples and further used as a reference for quantification of proteins in corresponding ghost samples.

### 2.4. PS and CD47

Phosphatidylserine (PS) exposure at the outer membrane leaflet of RBCs and CD47 were assessed using Annexin V-PE (Miltenyi, 130-118-363) and anti-CD47-PE antibody (Miltenyi 130-101-348), respectively. Briefly blood samples were centrifuged at  $1000 \times g$  for 5 min at RT. RBCs pellets were washed in PBS and resuspended at 0.2% Hct in the appropriate staining buffer according to manufacturer instructions. RBCs suspensions were incubated with Annexin-V-PE (1:11 dilution) or CD47-PE (1:34 dilution) for 20 min in the dark at RT. Unstained RBCs and isotype control (1:51 dilution, REA-PE, Miltenyi) were used as negative controls for PS exposure and CD47 levels, respectively. After incubation, samples were washed twice in their respective staining buffer and analyzed by flow-cytometry (MACSQuant Analyzer 10, Miltenyi). Gating was performed on 100,000 RBCs per condition.

### 2.5. RBCs-derived extracellular vesicles isolation and quantification

RBCs-derived extracellular vesicles (RBCs-EVs) were quantified as previously described<sup>19</sup>. RBCs-EVs were identified by Annexin-V-FITC (Beckman Coulter, IM3546), and anti-CD235a-PE antibody (Miltenyi, 130-100-259) co-labeling and quantified by flow cytometry. The Megamix Kit was used to standardize RBCs-EVs acquisition gate based on fluorescent microbead size (0.5, 0.9 and  $3 \mu\text{m}$ ; Biotec, 7801) according to the supplier's instructions. RBCs-EVs were defined as events that were both smaller than  $0.9 \mu\text{m}$  and positively labeled with both Annexin V-FITC and anti-CD235a-PE.

### 2.6. Metabolomic analysis

After production, samples were standardized at  $4 \times 10^6$  RBCs per  $\mu\text{L}$  and centrifuged at  $1500 \times g$  for 5 min at  $4^\circ\text{C}$ . RBCs pellets were collected and frozen at  $-80^\circ\text{C}$  pending analysis. Metabolites were analyzed by ultra-high-performance liquid chromatography–mass spectrometry (UHPLC–MS) as previously published<sup>20</sup>. Briefly, the analytical platform employs a Vanquish UHPLC system (Thermo Fisher Scientific, San Jose, CA, USA) coupled online to a Q Exactive mass spectrometer (Thermo Fisher Scientific). The (semi)polar extracts were resolved over a Kinetex C18 column,  $150 \text{ mm} \times 2.1 \text{ mm}$ ,  $1.7 \mu\text{m}$  particle size (Phenomenex, Torrance, CA, USA) equipped with a guard column (SecurityGuard™ Ultracartridge–UHPLC C18 for 2.1 mm ID Columns–AJO-8782–Phenomenex, Torrance, CA, USA) using an aqueous phase (A) of water and 0.1% formic acid and a mobile phase (B) of acetonitrile and 0.1% formic acid for positive ion polarity mode, and an aqueous phase (A) of water:acetonitrile (95:5) with 1 mmol/L ammonium acetate and a mobile phase (B) of acetonitrile:water (95:5) with 1 mmol/L ammonium acetate for negative ion polarity mode. The Q Exactive mass spectrometer (Thermo Fisher Scientific) was operated independently in positive or negative ion mode, scanning in Full MS mode (2 microscans) from 60 to  $900 m/z$  at  $70,000$  resolution, with 4 kV spray voltage, 45 sheath gas, and 15 auxiliary gas. Calibration was performed prior to analysis using the Pierce™ Positive and Negative Ion Calibration Solutions (Thermo Fisher Scientific). Acquired data

was then converted from raw to mzXML file format using Mass Matrix (Cleveland, OH, USA). Samples were analyzed in randomized order with a technical mixture injected after every 15 samples to qualify instrument performance. Metabolite assignments, isotopologue distributions, and correction for expected natural abundances of deuterium,  $^{13}\text{C}$ , and  $^{15}\text{N}$  isotopes were performed using MAVEN<sup>21</sup>. Discovery mode alignment, feature identification, and data filtering was performed using Compound Discoverer 2.0 (Thermo Fisher Scientific). Graphs, heat maps and statistical analyses, metabolic pathway analysis, PLS-DA and hierarchical clustering was performed using the MetaboAnalyst 4.0 package ([www.metaboanalyst.com](http://www.metaboanalyst.com))<sup>22</sup>.

### 2.7. Imaging-flow-cytometry

The proportion of discocytes, echinocytes, and spherocytes and parameters such as projected surface area, coefficient of area variation, perimeter and diameter were assessed using imaging flow cytometry (Amnis®, ImagestreamX, Merck). RBCs were diluted with AS3 to a final concentration of  $4.17 \times 10^6$  RBCs per mL. For each sample, around 100,000 images were captured at a low speed and high sensitivity fluidics mode and under  $60\times$  image magnification. An image segmentation template was designed on the IDEAS® software platform based on previous works<sup>23,24</sup>. Briefly, focused objects were identified by selecting images containing gradient root mean square (RMS) values above 49.62 (Gradient RMS\_M01\_BF1 from 82.16 to 49.62). Doublets and calibration beads images were removed using a plot of aspect ratio (Vertical Feature, Aspect Ratio\_M01) versus area (Horizontal Feature, Area\_M01) using the default bright field mask (Polygon Vertices: 28.34, 1.03, 130.28, 1.022, 92.27, 0.532, 50.8, 0.534). We then used a plot of area (Area\_M01 from 149.08 to 11.02) versus circularity (Circularity\_Object M01, BF1, Tight from 46.37 to 9.639) with the default bright field mask to select front RBCs images. Finally, during the experiment, we noticed a heterogeneity in the size and shape of RBCs flowing in front of the camera over time. In the first minutes, numerous small and irregular RBCs were observed, but their proportions stabilized over time. To overcome this issue, we decided to exclude the first 300 s of the acquisition from the analysis by plotting the area (Area\_Object M01, BF1, Tight from 114.64 to 7.879) versus time (from 300 to 891.41 s) for all samples. Different parameters were analyzed on selected RBCs such as area, coefficient of area variation, perimeter and diameter. Combined with hematological analysis of RBCs volume, projected surface area was used to measure of surface to volume ratio. Based on RBCs size we discriminated three RBCs sub-populations: small (Area\_Object M01, BF1, Tight from 42 to 0), intermediate (Area\_Object M01, BF1, Tight from 42 to 53) and big (Area\_Object M01, BF1, Tight from 53 to 130). Further analysis was performed to discriminate RBCs sub-populations based on morphological criteria. Briefly, RBCs corresponding to each of the categories of interest (discocytes, echinocytes, spherocytes) were hand-picked (at least 20 per structure), and the best feature finder tool was used to automatically identify the best parameters to discriminate these populations. Discocytes were identified by plotting H Variance Mean\_M01\_BF1\_15 (Horizontal Feature) against H Contrast Mean\_M01\_BF1\_15 (Vertical Feature) (Polygon Vertices: 23.15, 0.132, 13.73, 0.028, 8.926, 0.038, 2.509, 0.083, 10.5, 0.144, 23.74, 0.142) from the big RBCs sub-population. Spherocytes were identified by plotting H Variance Mean\_M01\_BF1\_15 (Horizontal Feature) against H Contrast Mean\_M01\_BF1\_15 (Vertical Feature) (Polygon Vertices: 8.522,

0.019, 4.797, 0.002, 3.843, 0.011, 6.384, 0.077, 10.41, 0.141, 11.44, 0.143, 21.9, 0.137, 13.23, 0.058) from remaining RBCs sub-populations (both small and intermediate sub-populations). All remaining focused, single cell, front view RBCs were considered as echinocytes. The relative proportions of discocytes as well as echinocytes and spherocytes categories were then analyzed for all samples.

### 2.8. Osmotic fragility

Osmotic fragility was assessed using Osmocell device (SD Medical) as previously described<sup>25</sup>. Briefly, blood samples were diluted (1/40) in 0.9% NaCl isotonic saline solution and analyzed using osmocell system. Salt concentration and hemolysis rate were calculated by the continuous measurement of conductance and blood light transmission, respectively. Osmotic fragility curve represents the percentage of light transmission against the conductance (g/L).

### 2.9. RBCs rheological properties

Osmotic ektacytometry gradient (*i.e.*, osmoscan; LORRCA MaxSis, RR Mechatronics) was used to evaluate the variation of RBCs deformability expressed as elongation index (EI) under constant shear stress (30 Pa) and osmolality gradient (50–500 mOsm/kg) as previously described<sup>19</sup>. The main parameters of the osmoscan curve determined were: 1) Omin; *i.e.*, the osmolality value at which EI reached the minimal value in the hypotonic zone of the gradient, which correlates with RBCs osmotic fragility and is affected by the surface to volume ratio, 2) EImax; *i.e.*, the maximum deformability of RBCs which is dependent on membrane deformability and cell surface, 3) Ohyper; *i.e.*, the osmolality value in the hypertonic arm of the osmoscan curve at which EI is half of EImax and which is related to the RBCs internal viscosity<sup>26,27</sup>. RBCs aggregability was determined at 37 °C by syllectometry method (LORRCA MaxSis), after adjustment of the Hct to 30% with PBS 1X + 3% dextran 70.

### 2.10. Mechanical retention

Microfiltration through microbeads mimicking the mechanical sensing of spleen was performed to quantify RBCs mechanical retention<sup>28</sup>. Five percent PKH67-stained proRBCs or eryaspase and 5% PKH26-stained pRBCs used as negative control were mixed to 90% non-stained pRBCs prior to injection into microfiltration system. The proportion of fluorescent RBCs was analyzed by flow cytometry (at least 10,000 events) before and after microfiltration to determine the percentage of mechanical retention.

### 2.11. RBCs survival and biodistribution in mice

All animal care and experimental procedures were in accordance with the French and European Regulations and NRC (National Research Council) Guide for the Care and Use of Laboratory Animals for animal housing and experimental procedures and with the European directive 2010/63/CE of the European Parliament and the Council, the decree n°2013 118 and decisions of February 1st, 2013 on the protection of animals used for scientific purposes. Male BALB/cByJ mice (10 weeks old) were purchased from Charles River Laboratories (France). Mice were housed

collectively in disposable standard cages in ventilated racks (A1 classified area) under a 12-h light, 12-h dark cycle with filtered water provided and irradiated standard laboratory food for rodent provided *ad libitum*. Mice were housed for at least 8 days before use in the experiments. Animals were euthanized under volatile anesthesia Isoflurane 1%–5%; oxygen 1–2 L/min by cervical dislocation.

Blood from healthy BALB/cByJ mice (Charles River Laboratories) was used to prepare mice surrogate products. Mice-eryaspase (m-eryaspase) was prepared as previously described<sup>29</sup> and mice-proRBCs (m-proRBCs) was prepared following the same procedure. Final products and non-processed mice RBCs (m-pRBCs) were adjusted to 50% Hct in SAG-mannitol, 20% decomplexed plasma. RBCs were labeled with DiR (DiOC<sub>18</sub>; ThermoFisher) dye and injected intravenously (IV) in healthy BALB/cByJ mice to evaluate their blood survival and biodistribution. Blood samples were collected at different time points (15 min, 1, 2, 3, 7, 10 and 20 days after injection) and the percentage of positive DiR RBCs was assessed by flow cytometry (FC500, Beckman Coulter). Fluorescence imaging of mice was performed before injection and 20 min, 1, 2, 3, 7, 10 and 20 days after injection with the optical imaging system IVIS Spectrum of PerkinElmer. A non-injected mouse was used as negative control. *In-vivo* fluorescence acquisition was performed on anaesthetized mice. Mice were induced and maintained under anesthesia with a mix of Isoflurane (1%–5%) and oxygen (1–2 L/min). The animals were placed in dorsal recumbency to obtain a ventral image. Semi quantitative analyze was performed in organs responsible for RBCs elimination (spleen, liver, bone marrow)<sup>30,31</sup> by placing a Region Of Interest (ROIs) on each organ in the ventral images. The fluorescence signal corresponding to the Total radiance efficiency was measured in each ROI. This protocol was approved by The VetAgro Sup ethical committee and by the “Ministère de l’Enseignement Supérieur et de la Recherche”. The ARRIVE guidelines were followed for the writing of this publication.

## 2.12. Statistical analysis

Kruskal-Wallis analysis followed by Dunn *post-hoc* tests were used for the comparison of hematological parameters, RBCs senescence markers, microfiltration, morphological, hemorheological and biodistribution features and one-way analysis of variance followed by Tukey *post-hoc* tests were used for the comparison of protein content and concentration between pRBCs, proRBCs and eryaspase samples. A  $P < 0.05$  was considered significant.

## 3. Results

### 3.1. Encapsulation process modulates RBCs volume with low impact on hemolysis

We first analyzed hematological parameters and observed that encapsulation process caused a significant decrease in mean corpuscular volume (MCV;  $-28\%$  and  $-25\%$  for proRBCs ( $P = 0.0009$ ) and eryaspase ( $P = 0.0048$ ), respectively; Fig. 1A). This reduction of MCV was associated with a significant decrease ( $P < 0.01$ ) in MCH ( $-21\%$  for both proRBCs and eryaspase) leading to a slight increase in mean corpuscular hemoglobin concentration (MCHC) after process, which was significant for proRBCs ( $P = 0.0001$ ) but not for eryaspase ( $P = 0.1138$ ) compared to pRBCs (Fig. 1B and C). RBCs distribution width increased in both proRBCs and eryaspase ( $P < 0.01$ ) compared to pRBCs (Fig. 1D). Slight but significant increases in free Hb level and hemolysis rate were observed in proRBCs and eryaspase compared to pRBCs with a level of hemolysis remaining below 2% (Fig. 1E and F;  $P < 0.01$ ). No significant difference was observed between eryaspase and proRBCs for hematological parameters.

### 3.2. Proteomic landscape is maintained after encapsulation process

We then performed mass spectrometry analysis of total and ghost RBCs allowing the identification and quantification of 1957 proteins; 1226 proteins in total RBCs and 1819 in

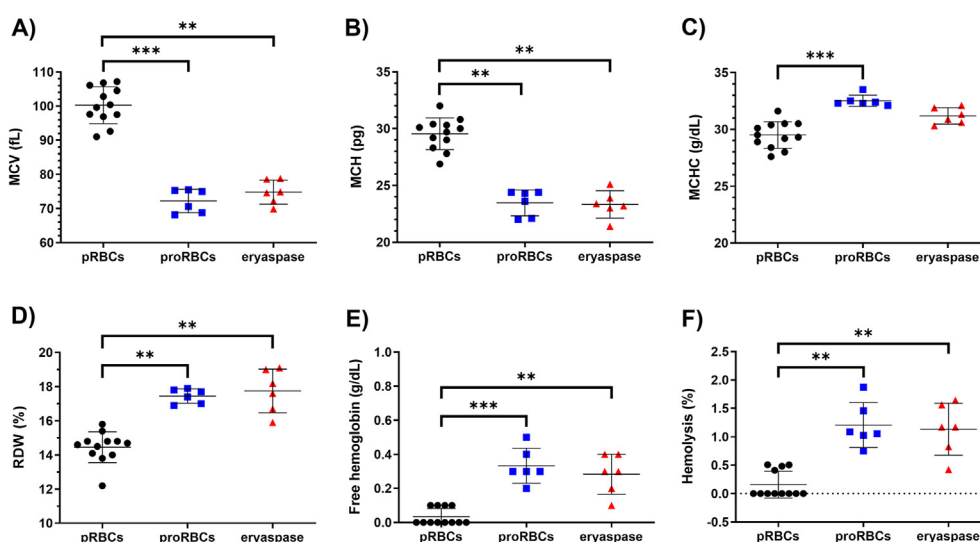


**Figure 1** Impact of encapsulation process on hematological parameters. Hematology analyzer was used to detect variations of (A) mean corpuscular volume (MCV), (B) mean corpuscular hemoglobin (MCH), (C) mean corpuscular hemoglobin concentration (MCHC), (D) RBCs distribution width (RDW), (E) free hemoglobin and (F) hemolysis percentage in proRBCs ( $n = 6$ ) eryaspase ( $n = 6$ ) as well as corresponding pRBCs ( $n = 12$ ) samples. Horizontal lines represent mean values  $\pm$  SD of the indicated number of analyzed samples. Significantly different from pRBCs: \* $P < 0.05$ , \*\* $P < 0.01$ , \*\*\* $P < 0.001$ .

ghost RBCs. The content of each protein detected was compared between each pair of samples using Pearson correlation. We observed strong correlations between each pair of samples, ( $R$  ranging between 0.94 and 0.98 for total and ghost RBCs, respectively, Fig. 2). Unsupervised hierarchical clustering analysis was then performed to compare the proteomic profiles between samples. Global proteomic profiles were very similar between pRBCs, proRBCs and eryaspase, in both total and ghost RBCs, demonstrating a low variability of protein content after encapsulation process with or without ASNase (Fig. 3A). In addition, by looking at some key cytosolic, membrane, and cytoskeleton proteins we observed that their content were similar in all samples (Fig. 2). Finally, after application of 1% false discovery rate, statistical analysis revealed that only ASNase content was significantly different between eryaspase ( $q$ -value = 0.079) and pRBCs or proRBCs. Related to the observed decrease in MCH after encapsulation process, we also observed a decrease in total protein content: from 39.0 pg for pRBCs to 31.2 and 32.1 pg for proRBCs ( $P = 0.0059$ ) and eryaspase ( $P = 0.0005$ ), respectively. Nevertheless, the total protein concentration was not different ( $P > 0.05$ ) between the three types of RBCs (411 mg/mL for pRBCs, 421 mg/mL for proRBCs and 421 mg/mL for eryaspase). Lastly, principal component analysis indicated that the difference observed in RBCs proteomic profile was higher between pRBCs from different blood donors than between one pRBCs and the corresponding proRBCs and eryaspase (Fig. 3B).

### 3.3. Encapsulation process promotes RBCs-EVs release without severe changes in other RBCs senescence markers

We further used flow cytometry to analyze RBCs senescence markers and observed that the encapsulation process promoted RBCs-EVs release in both eryaspase ( $P = 0.025$ ) and proRBCs ( $P = 0.004$ ) compared to pRBCs (Table 1). No significant difference in CD47 level was observed between all samples (Table 1;  $P = 0.99$ ). While we observed a slight increase of PS-exposing RBCs in both proRBCs and eryaspase compared to pRBCs ( $P = 0.0083$  and  $0.0231$ , respectively), its levels remained rather low in all conditions ( $<1.1\%$ ). No significant difference in the percentage of RBCs expressing PS, RBCs-EVs concentration and CD47 level were observed between proRBCs and eryaspase.

### 3.4. Encapsulation process decreases metabolite content and activates the pentose phosphate pathway

UHPLC coupled to MS allowed the detection of 177 metabolites in RBCs pellets. In line with proteomics results, metabolomic experiments showed a decrease of intracellular metabolites content after encapsulation process. As suggested by volcano plot analysis, the RBC metabolomic profile was modified after encapsulation process (Fig. 4A) with most amino acids being significantly depleted. Only few amino acids were not, or only slightly impacted such as phenylalanine, glycine and cysteine. Interestingly, compared to proRBCs, eryaspase samples showed

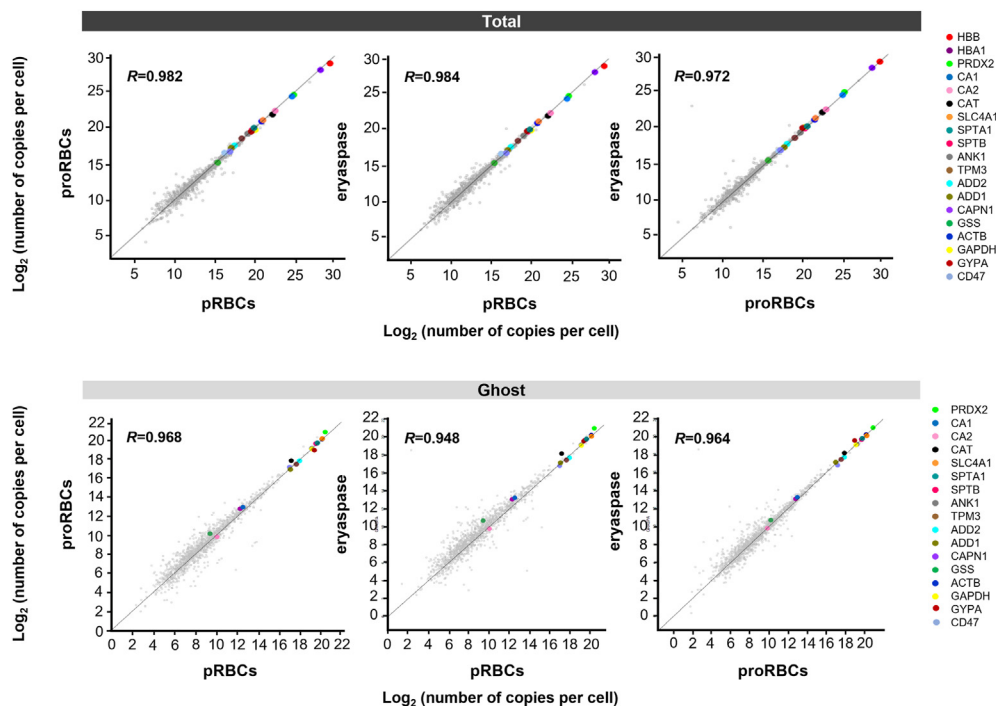


**Figure 2** Comparison of the amount of each protein detected in RBCs, before and after encapsulation process, and with or without asparaginase (ASNase). The number of copies per cell of the proteins identified in pRBCs, proRBCs, eryaspase ( $n = 4$  per group) was compared between each pair of samples using a scatter plot. The Pearson correlation coefficient ( $R$ ) was calculated for comparisons between all samples. Data for total and ghosts RBCs were separated. Some key RBCs proteins were displayed: hemoglobin proteins (HBB, HBA1), peroxiredoxin 2 (PRDX2), carbonic anhydrase (CA1, CA2), catalase (CAT), band 3 anion exchanger (SLC4A1), alpha and beta spectrin (SPTA1 and SPTB), ankyrin (ANK1), tropomyosin (TPM3), alpha and beta adducin (ADD1 and ADD2), calpain 1 catalytic subunit (CAPN1), glutathione-S-synthetase (GSS), actin (ACTB), glyceraldehyde-3-phosphate-dehydrogenase (GAPDH), Glycophorin A (GYPA), CD47.

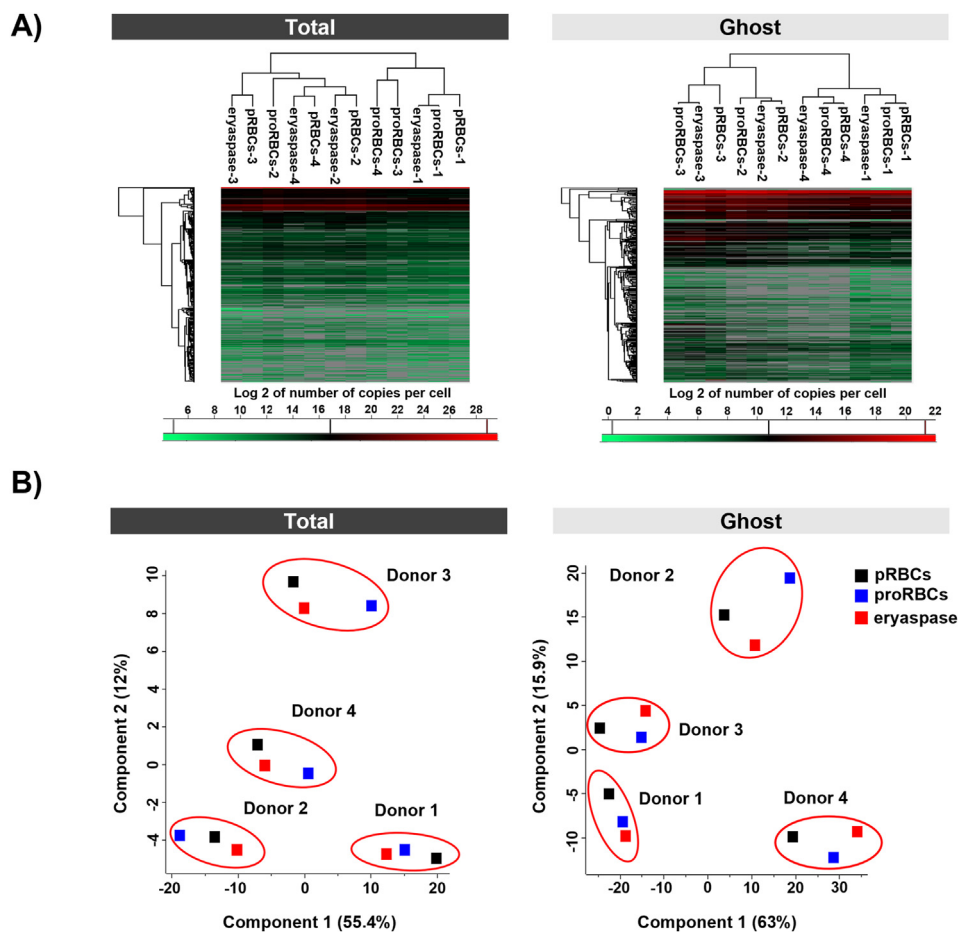


**Figure 3** Proteomic profile before and after encapsulation process with or without ASNase. (A) Hierarchical clustering analysis was performed on  $\log_2$  of the proteins (number of copies per cell) in total and ghost samples. The heat map represents highly expressed proteins in red, lowly expressed proteins in green and undetected proteins in gray. The dendrograms on top show the hierarchical clustering of the different samples analyzed (Euclidean distances). (B) Principal component analysis was performed on  $\log_2$  of the proteins (number of copies per cell) detected in the 3 conditions in total RBCs samples and ghost samples. Significantly different from pRBCs: \* $P < 0.05$ , \*\* $P < 0.01$ , \*\*\* $P < 0.001$ .

a significant decrease in asparagine ( $P = 0.01$ ) and glutamine ( $P = 0.02$ ) combined with an increase in glutamate ( $P = 0.04$ ) demonstrating ASNase activity inside RBCs (Fig. 4B). We also observed a decrease in glutathione in processed RBCs with and without ASNase, which may be due to impaired biosynthesis in line with the decrease in amino acids content and supported by the lack of oxoproline accumulation (glutathione recycling

metabolite; Fig. 4B). As glutathione biosynthesis is an ATP dependent process, we observed decreased levels of ATP, which is produced during late glycolysis in RBCs. Accordingly, the levels of late glycolytic intermediates and end-product lactate were decreased, while the levels of early glycolytic metabolites were increased. In addition, accumulation of pentose phosphate pathway (PPP) intermediates was also evident, indicating

**Table 1** PS exposure, CD47 expression and RBCs-EVs release before and after encapsulation process.

Sample	Phosphatidylserine exposure (%)	CD47 expression (MFI)	RBCs-derived EVs [C]/ $\mu$ L
pRBCs	0.09 ( $\pm 0.02$ )	3.97 ( $\pm 0.52$ )	158 (IQR 99–379)
<i>n</i>	10	12	12
proRBCs	0.55 ( $\pm 0.49$ )**	4.17 ( $\pm 0.43$ )	3554 (IQR 1579–5687)**
<i>n</i>	5	6	6
Eryaspase	0.33 ( $\pm 0.14$ )*	3.78 ( $\pm 0.55$ )	2393 (IQR 290–13,017)*
<i>n</i>	5	6	6

Flow cytometry analysis was used to detect the variation in percentage of cells with phosphatidylserine exposure at the membrane; mean fluorescence intensity (MFI) of CD47-positive-cells and RBCs-EVs content per  $\mu$ L in proRBCs ( $n = 6$ ), eryaspase ( $n = 6$ ) as well as corresponding pRBCs ( $n = 12$ ) samples. Data of PS exposure and CD47 expression are represented as mean values  $\pm$  SD of the indicated number of analyzed samples. Data of RBCs-derived EVs are represented as median value and interquartile range (IQR). Significantly different from pRBCs: \* $P < 0.05$ , \*\* $P < 0.01$ , \*\*\* $P < 0.001$ .

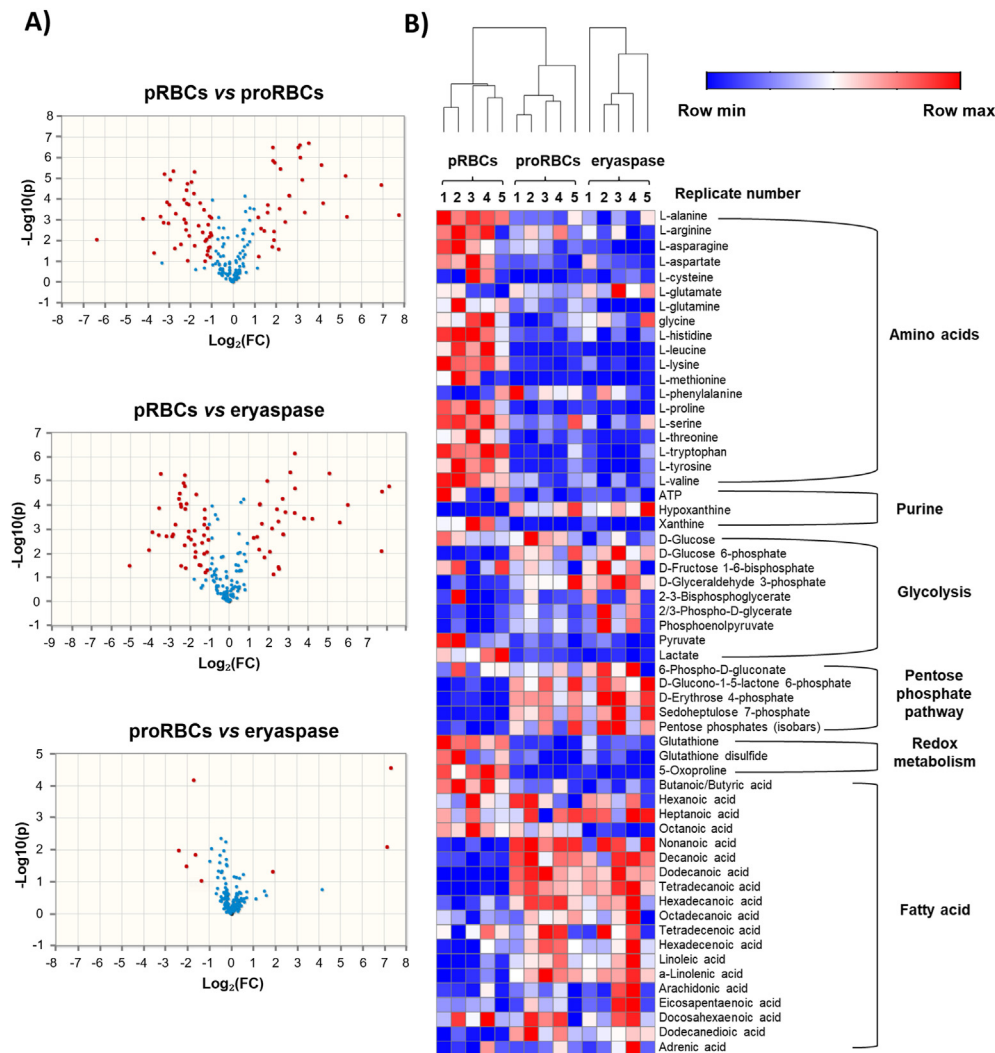


**Figure 4** Effects of encapsulation process on RBCs metabolome. (A) Volcano plot analysis of RBCs metabolites. Fold changes and  $P$ -values are pictured as Volcano plots with individual comparisons between pRBCs, proRBCs and eryaspase samples ( $n = 5$  per group). Metabolites with a magnitude fold change  $>2$  and a  $-\log_{10}(P\text{-value}) >1$  are plotted in red. (B) Hierarchical clustering of the main RBCs metabolic pathways and metabolites in pRBCs, proRBCs and eryaspase samples. Heat map represents normalized quantitative values which are represented by a color gradient (blue to red: minimum to maximum expression).

activation of the PPP. Finally, we also observed increased levels of free fatty acids after encapsulation process, suggesting lipid remodeling (Fig. 4B).

### 3.5. Encapsulation process increases the percentage of echinocytes without any change in RBCs surface area

Using imaging flow cytometry, we investigated the impact of encapsulation process on RBCs morphology. We observed a 15% increase in echinocytic-like shapes in both proRBCs and eryaspase compared to pRBCs ( $P < 0.05$  and  $P < 0.01$ , respectively) (Fig. 5A and B). As a consequence, the proportion of discocytes decreased in proRBCs and eryaspase samples whereas the proportion of spherocytes was similar in all samples (Fig. 5B). Interestingly, although cell volume decreased after encapsulation process, the projected surface area, perimeter and diameter of the cells were not affected ( $P = 0.999$ , Fig. 5C). The coefficient of

variation of area ( $P < 0.01$ ) was increased, which confirms higher RBCs size heterogeneity after process.

### 3.6. Encapsulation process changes RBCs deformability but has no impact on their mechanical retention

We explored RBCs rheology and observed that after encapsulation process, the osmoscan curves for both eryaspase and proRBCs were shifted to the left compared to pRBCs curves (Fig. 6A). Indeed, Ohyper decreased in both proRBCs ( $P < 0.0001$ ) and eryaspase ( $P = 0.04$ ) compared to pRBCs (Fig. 5B), demonstrating RBCs dehydration and increased internal viscosity. These results are in line with the decreased MCV and increased MCHC observed after encapsulation process (Fig. 1). The shift of the osmoscan curves to the left for proRBCs and eryaspase samples led to a decrease of Omin, which was no longer detectable (Fig. 6A), suggesting an increased surface area to volume ( $S/V$ ) ratio and a decrease in osmotic fragility<sup>26</sup>. The maintained

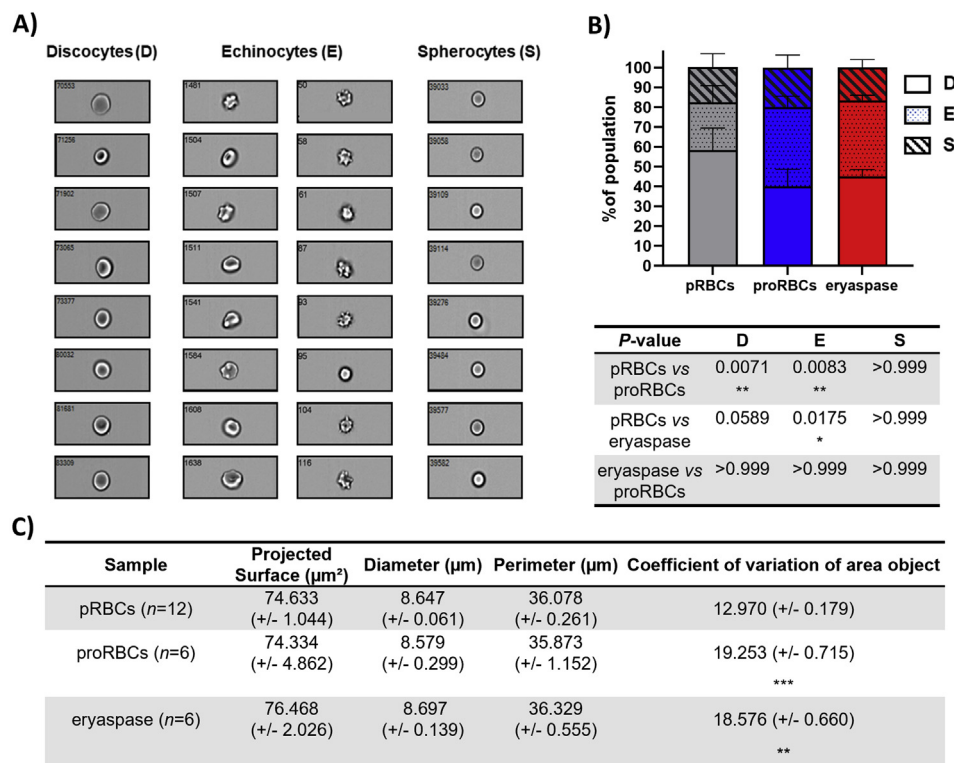


**Figure 5** Effect of encapsulation process on RBCs morphological parameters. Imaging flow cytometry was used to analyze RBCs morphology. For each sample, around 100,000 images were captured at a low speed and high sensitivity fluidics mode and under  $60\times$  image magnification. (A) RBCs were discriminated into the following morphological categories: discocytes, echinocytes (without discrimination between types I, II, III) and spherocytes. (B) The percentage of the different RBCs morphological populations: discocytes, echinocytes, spherocytes and (C) the surface, diameter, perimeter and coefficient of variation of area object were determined in proRBCs ( $n = 6$ ), eryaspase ( $n = 6$ ) as well as corresponding pRBCs ( $n = 12$ ) samples. Data represent mean values  $\pm$  SD of the indicated number of analyzed samples. Significantly different from pRBCs: \* $P < 0.05$ , \*\* $P < 0.01$ , \*\*\* $P < 0.001$ .

projected area (Fig. 5C) associated to the decrease of MCV (Fig. 1A) after encapsulation process led to a 1.4-fold increase of their  $S/V$  ratio ( $P < 0.01$ ) (Fig. 6B). Osmotic fragility analysis confirmed the improved resistance to osmotic stress in processed RBCs with a decrease of 46% and 56% of osmotic fragility for eryaspase ( $P = 0.0184$ ) and proRBCs ( $P = 0.0007$ ), respectively (Fig. 6C). The maximum deformability ( $EI_{\text{max}}$ ) of processed RBCs occurred at lower osmolality and was slightly lower compared to pRBCs ( $-11\%$  and  $-15\%$  in eryaspase and proRBCs, respectively; Fig. 6A and C). No significant difference in RBCs aggregation was observed between pRBCs, eryaspase and proRBCs (Fig. 6B). Finally, by using an *in vitro* splenic microfiltration model, we observed no mechanical retention of proRBCs and eryaspase by the meshwork of beads with a percentage of RBCs recovery similar in all samples (Fig. 6D).

### 3.7. Encapsulation process has no major impact on RBCs circulation half-life in mouse model

Surrogate mice RBCs products were used to assess processed RBCs behavior *in vivo*. The m-eryaspase and m-proRBCs samples had decreased MCV, osmotic fragility, and a shift of the osmoscan curves to the left (Supporting Information). Blood elimination rate of processed RBCs ( $-19.2\%$  and  $-26.9\%$  for m-eryaspase ( $P = 0.069$ ) and m-proRBCs ( $P = 0.0020$ ), respectively) at 24 h post injection was 4–5 times higher compared to m-pRBCs

( $-5\%$ ; Fig. 7A). After 24 h and until 20 days, m-proRBCs and m-eryaspase displayed the same trend of blood elimination than m-pRBCs with a percentage of RBCs loss of 71.53% for m-pRBCs, 75.13% for m-eryaspase and 79.18% for m-proRBCs ( $P = 0.0029$ , Fig. 7A). Overall the half-life of m-proRBCs and m-eryaspase was  $13.0 \pm 4.5$  and  $15.1 \pm 1.5$  days in mouse, respectively, compared to  $20.8 \pm 10.9$  days for m-pRBCs with no significant difference between the three conditions. The overall biodistribution and the semi-quantitative analysis in spleen, liver and bone marrow using fluorescent imaging did not show any difference of distribution over time between the different RBCs (Supporting Information, Fig. 7B).

## 4. Discussion

While RBCs have been identified as promising drug carriers and are currently being investigated in clinical trials for several indications, improvement of the knowledge concerning the impact of hypotonic dialysis on RBCs properties is necessary to accelerate the development of new RBCs-based therapies. In the present study, we combined a wide panel of techniques (molecular, cellular, metabolomic, proteomic, morphology, red blood cell rheology as well as *in vivo* biodistribution) in an effort to fully characterize RBCs after hypotonic dialysis using ERYCAPS® encapsulation technology. To our knowledge, this is the first time such a full and in-depth analysis was performed to characterize

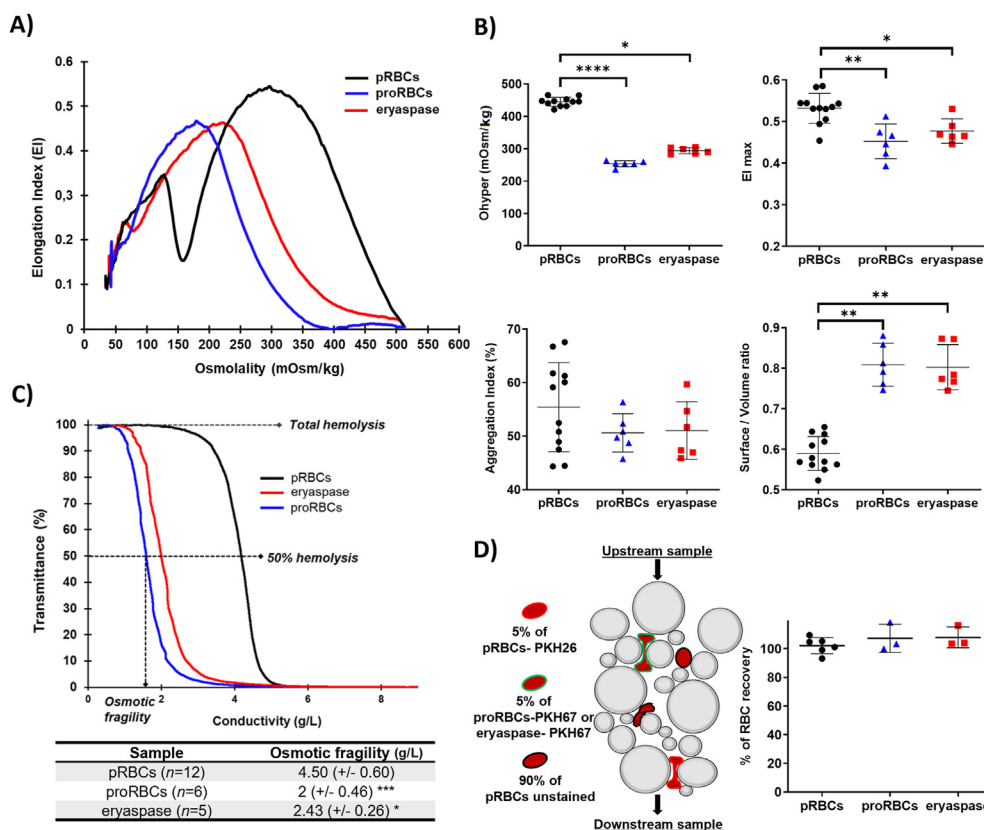


**Figure 6** Effect of encapsulation process on hemorheological parameters and mechanical retention using an *in vitro* splenic microfiltration model. (A) Representative osmoscan curve of pRBCs, proRBCs, eryaspase. (B) Comparison of Ohyper, Elmax values of osmoscan curves, of the percentage of aggregation, and of the *S/V* ratio value for all samples. (C) Representative curve of osmotic fragility and summary table of the mean  $\pm$  standard deviation osmotic fragility in proRBCs ( $n = 6$ ), eryaspase ( $n = 5$ ) and pRBCs ( $n = 12$ ) samples. (D) Representative schema of the *in vitro* splenic microfiltration model used and the conditions tested. The percentage of recovery of proRBCs ( $n = 3$ ), eryaspase ( $n = 3$ ) as well as corresponding pRBCs ( $n = 6$ ) in downstream sample were determined by flow cytometry. Horizontal lines represent mean values  $\pm$  standard deviation of the indicated number of analyzed samples. Significantly different from pRBCs: \* $P < 0.05$ , \*\* $P < 0.01$ , \*\*\* $P < 0.001$ , \*\*\*\* $P < 0.0001$ .

RBCs after hypotonic dialysis to ensure their efficacy and safety as drug carriers. Our key findings showed that the ERYCAPS® hypotonic dialysis-based RBCs encapsulation process was accompanied by: 1) a reduction of intracellular content without any alteration in the proteomic profile, 2) a change in RBCs rheology and shape distribution without any significant impact on mechanical retention through a spleen mimicking device, 3) metabolic modifications through activation of the PPP and 4) a moderate release of RBCs-EVs. The encapsulation process also increased the *S/V* ratio of RBCs, improving their resistance to osmotic stress. Finally, the half-life of murine RBCs was not significantly affected by encapsulation process in mice.

ProRBCs and eryaspase samples exhibited similar changes for nearly all parameters analyzed compared to unprocessed RBCs, indicating that these differences were primarily due to the encapsulation process and not the addition of ASNase. And where eryaspase did differ significantly from proRBCs, it was attributable to the activity of ASNase, which reduced the levels of both asparagine and glutamine and increased the level of glutamate.

Altogether, proteomic and metabolomic results suggest a loss of intracellular content induced by the encapsulation process. This reduction seems to be an inherent consequence of osmotic-encapsulation processes, in line with previous studies reporting a

decrease in MCH after hypotonic-dialysis<sup>9–13,32–34</sup>. While the formation of transient pores is required for drugs to diffuse inside RBCs, these pores can also allow a portion of the intracellular contents to leak out. Indeed, the decrease in MCV and the left-shift of the osmoscan curve in both proRBCs and eryaspase strongly suggest RBCs dehydration after the encapsulation process, as previously shown by other groups<sup>11–13,32,35–37</sup>. Interestingly, although the results were not statistically significant, proRBCs displayed a lower Ohyper value and higher MCHC than eryaspase suggesting slightly greater RBCs dehydration in proRBCs samples. These results suggest that the loading of ASNase in RBCs would compensate for the loss of some of the intracellular content by maintaining osmotic balance to some extent. Our results also confirmed that RBCs dehydration after the encapsulation process increased RBCs size heterogeneity<sup>34</sup>. Yet despite this dehydration, the activation of the phosphate pentose pathway and the maintenance of glycolytic metabolites demonstrate that RBCs remain metabolically active after the encapsulation process. Furthermore, since the decrease in RBCs volume was accompanied by a reduction in intracellular content, protein concentration remained substantially similar among pRBCs, proRBCs and eryaspase.

RBC deformability was decreased after the encapsulation process. This reduction can be attributed to the RBCs dehydration

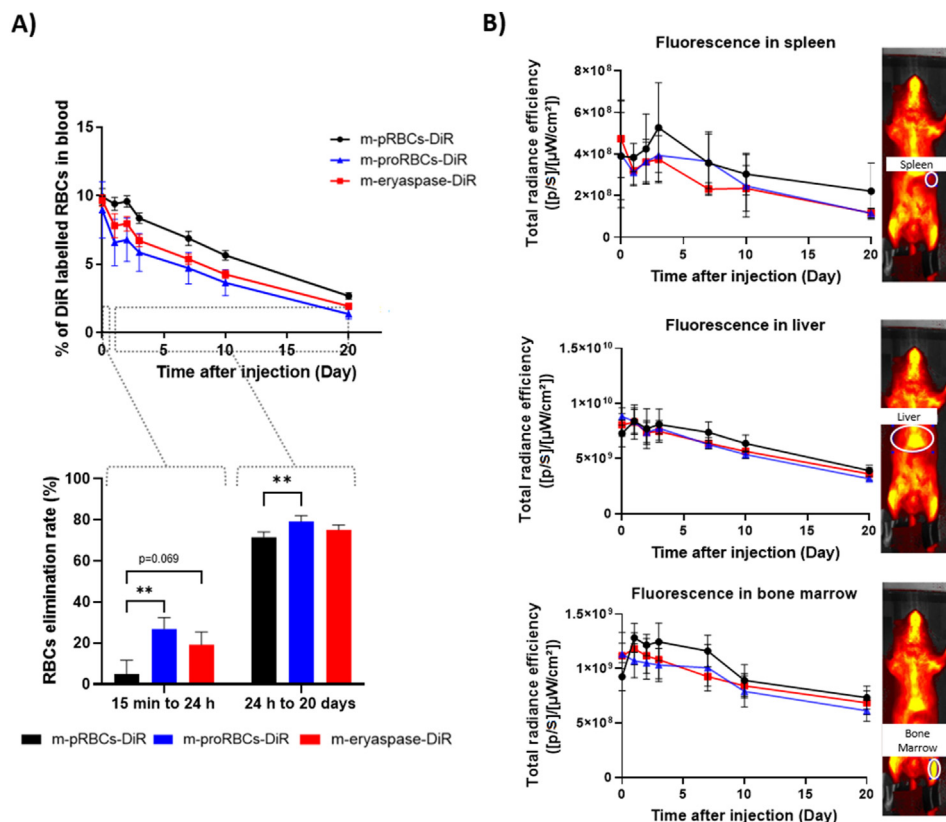


**Figure 7** Effect of encapsulation process on *in vivo* RBCs biodistribution in mice. m-pRBCs m-proRBCs and m-eryaspase labeled with DiR were injected IV in BALB/cByJ mice ( $n = 6$  for each group) to evaluate their blood survival by flow cytometry and biodistribution by fluorescent imaging. (A) The percentage of RBCs-DiR in blood was determined over 20 days. The elimination rate of RBCs-DiR was calculated between 15 min and 24 h and between 24 h and 20 days. (B) Total radiance efficiency of DiR fluorescence in spleen, liver and bone marrow was determined in mice. Images illustrating ROI position for each organ of interest was represented on the right. Data represent mean values  $\pm$  SD of the indicated number of analyzed samples. Significantly different from m-pRBCs: \* $P < 0.05$ , \*\* $P < 0.01$ , \*\*\* $P < 0.001$ .

and the increase of internal viscosity<sup>38</sup>. In addition, the rise in fatty acid content and the higher amount of RBCs-EVs released by processed RBCs suggest lipid and membrane remodeling, which could have also contributed to the reduction of RBC deformability. Normally, RBCs with reduced deformability are retained by the spleen and eliminated from the bloodstream<sup>39</sup>. However, the results obtained with the splenic microfiltration model do not support a higher mechanical retention of processed RBCs compared to pRBCs. In the mouse model, larger amount of m-proRBCs and m-eryaspase are eliminated from circulation during the first 24 h after injection suggesting the elimination of the most fragile RBCs. However, the overall half-life of the surrogate mouse product was not significantly different in mice compared to pRBCs suggesting that the encapsulation process does not substantially affect RBCs survival. Further, the 18–20 days mean terminal half-life of ASNase in eryaspase (observed in the phase I clinical study) supports the ability of processed RBCs to circulate for a long period of time. Previous studies using the splenic microfiltration model demonstrated that a decrease in the RBCs  $S/V$  ratio may result in elevated mechanical retention, while a decrease in RBCs membrane elasticity/deformability only cause a slight increase of mechanical retention<sup>40–42</sup>. Thus, the *in vivo* persistence of processed RBCs in mouse and human despite their altered rheological properties could be explained in part by the increased  $S/V$  ratio, or at least by its maintenance, after the

encapsulation process. Finally, the low level of hemolysis (*e.g.*,  $<2\%$ ) and the decreased osmotic fragility of both proRBCs and eryaspase suggest that RBCs are not made dramatically more fragile by the encapsulation process. Another hypothesis is that the most fragile RBCs would hemolyze during the encapsulation procedure, leading to the enrichment of the most resistant RBCs which would persist in the blood circulation for almost the same time compared to non-processed RBCs.

Previous studies showed that osmotic encapsulation methods promoted alterations in the shape of RBCs, including the formation of echinocytes and spherocytes<sup>9,14,15,34,35</sup>. We determined that 15% of processed RBCs became echinocytic whereas the proportion of spherocytes was not changed. And while the spherocytic shape is irreversible, it has been demonstrated that echinocytes may revert to discocytes under certain conditions<sup>43</sup>. Echinocytes are characterized by spicules at the RBCs membrane which can bud to form extracellular vesicles<sup>44,45</sup>. Furthermore, oxidative stress, is also known to trigger RBCs vesiculation<sup>46</sup> and could be involved in the increased release of RBCs-EVs after encapsulation process. It should be noted, however, that the measured RBCs-EVs levels were still within the range of those observed in standard stored concentrates<sup>24,47–50</sup>.

Although the percentage of PS-exposing cells remained rather low ( $<1.1\%$ ) its increase after encapsulation process could be the result of oxidative damage, which is known to generate membrane

phospholipid asymmetry disruption<sup>51</sup>. Moreover, the increase of fatty acid content and RBCs hemolysis suggests an increase of oxidative stress in RBCs after the encapsulation process. The decreased glutathione pool after encapsulation may be due to the depletion of cysteine, which is the rate-limiting substrate for glutathione biosynthesis. In addition, as this process is ATP dependent, we observed a blockade in glycolysis, with decreased levels of late-stage and increased levels of early-stage glycolytic intermediates. This blockade could occur through oxidation of functional cysteine residues in GAPDH, a process which occurs in settings of increased oxidative stress in RBCs<sup>52</sup>. In support of this possibility, PPP activation suggests increased NADPH production to reduce GSSG back to GSH, in order to compensate as much as possible for the enhanced oxidative stress to reduce RBCs alterations.

The persistence of processed RBCs in the bloodstream after infusion hints at an under-appreciated ability of ERYCAPS®-processed RBCs to adapt their metabolism and, more broadly, to reverse alterations associated with hypotonic dialysis-based encapsulation. Indeed, several changes are reported to be reversible after packed RBCs transfusion, including intracellular ATP content, which recovers within a few hours after transfusion<sup>53</sup>. Furthermore, the use of new preservative solutions with basic pH<sup>54,55</sup> or a rejuvenation solution could be used to reactivate the energy-generating and antioxidant pathways<sup>56</sup>, reduce intracellular calcium, decrease reactive oxygen species and PS exposure, help in the recovery of deformability<sup>57,58</sup> and limit the release of RBCs-EVs<sup>59</sup>. In any case, once the processed RBCs are infused into the bloodstream, their long half-life suggests that they may have functional glycolysis, intact antioxidant defenses and normal plasticity. Mechanistically, processed cells might restore levels of ATP and amino acids, which could allow them to regenerate their glutathione pool and antioxidant defenses. Nevertheless, irreversible changes, such as membrane asymmetry disruption and RBCs-EVs release, could explain the slight, although not significant, decrease in half-life compared to unprocessed RBCs. However, for drug carrier purposes, processed RBCs duration in the bloodstream is sufficient to prolong ASNase terminal half-life from 1.3 days (free ASNase) to 18–20 days (encapsulated ASNase).

## 5. Conclusions

In conclusion, a full and in-depth characterization of the physiological, biophysical, metabolomic, proteomic and cellular properties of RBCs after drug loading was performed. This wide characterization allowed to have a systemic and integrative approach to demonstrate that ERYCAPS® hypotonic dialysis encapsulation process induces some changes to RBCs features without substantially affecting their survival or their capacity to carry therapeutics making them suitable as drug carriers. These results are consistent with our previous findings that demonstrated the superior safety, pharmacokinetic, and pharmacodynamic profile of RBCs encapsulating ASNase compared to free ASNase. Further studies are needed to characterize the therapeutic-encapsulated RBCs in physiological environments, to better understand how they remain viable and metabolically active in the bloodstream after infusion.

## Acknowledgments

The Orbitrap Fusion mass spectrometer was acquired at 3P5 proteom'IC facility with funds from the FEDER through the

Operational Programme for Competitiveness Factors and Employment 2007–2013 (France), and from the Cancéropôle Ile de France (France). The authors would like to thank manufacturing department, industrial transfer unit and industrial development unit for the production of the batches (Erytech Pharma); Aurély Andrivon, Aurore Cléret and Caroline Desvignes for operational and technical assistance for *in vivo* studies (Erytech Pharma); Emmanuel Chereul, Marie Foskolos and their team for animal care and follow-up of the *in vivo* studies (VOXCAN, Marcy l'Etoile, France); Sébastien Dussurgey and Thibault Andrieu for imaging flow cytometry (AniRA-Cytometry facility); François Guillonnet for proteomic study (3P5 proteom'IC facility).

## Author contributions

Mélanie Robert, Bastien Laperrousaz, Diana Piedrahita, Emilie-Fleur Gautier, Elie Nader, Florian Dupuy, Travis Nemkov, Virginie Salnot performed experiments and analyzed data; Patrick Mayeux, Angelo D'Alessandro, Catherine Lavazec, Philippe Joly, Philippe Connes analyzed data; Alexander Scheer originated the idea for the study, Agnès Cibiel designed the study and analyzed data. Mélanie Robert, Philippe Connes, Agnès Cibiel wrote the manuscript and all the authors reviewed the manuscript.

## Conflicts of interest

Agnès Cibiel, Alexander Scheer, Bastien Laperrousaz, Diana Piedrahita and Mélanie Robert are employees of Erytech Pharma. Other authors declare no conflict of interest.

## Appendix A. Supporting information

Supporting data to this article can be found online at <https://doi.org/10.1016/j.apsb.2021.10.018>.

## References

- Rossi L, Serafini S, Pierigé F, Antonelli A, Cerasi A, Fraternali A, et al. Erythrocyte-based drug delivery. *Expert Opin Drug Deliv* 2005; **2**:311–22.
- Hamidi M, Zarrin A, Foroozesh M, Mohammadi-Samani S. Applications of carrier erythrocytes in delivery of biopharmaceuticals. *J Control Release* 2007; **118**:145–60.
- Patel PD, Dand N, Hirlekar RS, Kadam VJ. Drug loaded erythrocytes: as novel drug delivery system. *Curr Pharm Des* 2008; **14**:63–70.
- He H, Ye J, Wang Y, Liu Q, Chung HS, Kwon YM, et al. Cell-penetrating peptides mediated encapsulation of protein therapeutics into intact red blood cells and its application. *J Control Release* 2014; **176**:123–32.
- Dong Q, Jin W. Monitoring diclofenac sodium in single human erythrocytes introduced by electroporation using capillary zone electrophoresis with electrochemical detection. *Electrophoresis* 2001; **22**:2786–92.
- Lizano C, Sanz S, Luque J, Pinilla M. In vitro study of alcohol dehydrogenase and acetaldehyde dehydrogenase encapsulated into human erythrocytes by an electroporation procedure. *Biochim Biophys Acta* 1998; **1425**:328–36.
- Piergiorganni M, Casagrande G, Taverna F, Corridori I, Frigerio M, Bianchi E, et al. Shear-induced encapsulation into red blood cells: a new microfluidic approach to drug delivery. *Ann Biomed Eng* 2020; **48**:236–46.

8. Bourgeaux V, Lanao JM, Bax BE, Godfrin Y. Drug-loaded erythrocytes: on the road toward marketing approval. *Drug Des Devel Ther* 2016;**10**:665–76.
9. Hamidi M, Azimi K, Mohammadi-Samani S. Co-encapsulation of a drug with a protein in erythrocytes for improved drug loading and release: phenytoin and bovine serum albumin (BSA). *J Pharm Pharm Sci* 2011;**14**:46–59.
10. Mambrini G, Mandolini M, Rossi L, Pierigè F, Capogrossi G, Salvati P, et al. *Ex vivo* encapsulation of dexamethasone sodium phosphate into human autologous erythrocytes using fully automated biomedical equipment. *Int J Pharm* 2017;**517**:175–84.
11. Sanz S, Lizano C, Luque J, Pinilla M. *In vitro* and *in vivo* study of glutamate dehydrogenase encapsulated into mouse erythrocytes by a hypotonic dialysis procedure. *Life Sci* 1999;**65**:2781–9.
12. Antonelli A, Pacifico S, Sfara C, Tamma M, Magnani M. Ferucarbotran-loaded red blood cells as long circulating MRI contrast agents: first *in vivo* results in mice. *Nanomedicine (Lond)* 2018;**13**:675–87.
13. Chen ZA, Wu S-H, Chen P, Chen YP, Mou CY. Critical features for mesoporous silica nanoparticles encapsulated into erythrocytes. *ACS Appl Mater Interfaces* 2019;**11**:4790–8.
14. Sternberg N, Georgieva R, Duft K, Bäuml H. Surface-modified loaded human red blood cells for targeting and delivery of drugs. *J Microencapsul* 2012;**29**:9–20.
15. Favretto ME, Cluitmans JCA, Bosman GJCGM, Brock R. Human erythrocytes as drug carriers: loading efficiency and side effects of hypotonic dialysis, chlorpromazine treatment and fusion with liposomes. *J Control Release* 2013;**170**:343–51.
16. Domenech C, Thomas X, Chabaud S, Baruchel A, Gueyffier F, Mazingue F, et al. L-Asparaginase loaded red blood cells in refractory or relapsing acute lymphoblastic leukaemia in children and adults: results of the GRASPALL 2005-01 randomized trial. *Br J Haematol* 2011;**153**:58–65.
17. Hammel P, Fabienne P, Mineur L, Metges J-P, Andre T, De La Fouchardiere C, et al. Erythrocyte-encapsulated asparaginase (eryaspase) combined with chemotherapy in second-line treatment of advanced pancreatic cancer: an open-label, randomized Phase IIb trial. *Eur J Cancer* 2020;**124**:91–101.
18. Gautier E-F, Leduc M, Cochet S, Bailly K, Lacombe C, Mohandas N, et al. Absolute proteome quantification of highly purified populations of circulating reticulocytes and mature erythrocytes. *Blood Adv* 2018;**2**:2646–57.
19. Nader E, Monedero D, Robert M, Skinner S, Stauffer E, Cibiel A, et al. Impact of a 10 km running trial on eryptosis, red blood cell rheology, and electrophysiology in endurance trained athletes: a pilot study. *Eur J Appl Physiol* 2020;**120**:255–66.
20. Nemkov T, Reisz JA, Gehrke S, Hansen KC, D'Alessandro A. High-throughput metabolomics: isocratic and gradient mass spectrometry-based methods. *Methods Mol Biol* 2019;**1978**:13–26.
21. Clasquin MF, Melamud E, Rabinowitz JD. LC–MS data processing with MAVEN: a metabolomic analysis and visualization engine. *Curr Protoc Bioinformatics* 2012;**37**:14.11.1–23.
22. Chong J, Soufan O, Li C, Caraus I, Li S, Bourque G, et al. MetaboAnalyst 4.0: towards more transparent and integrative metabolomics analysis. *Nucleic Acids Res* 2018;**46**:W486–94.
23. Application of image flow cytometry for the characterization of red blood cell morphology. In: Pinto RN, Sebastian JA, Parsons M, Chang TC, Acker JP, Kolios MC, et al., editors. Proceedings of SPIE 10076, High-speed biomedical imaging and spectroscopy: toward big data instrumentation and management II, 100761F; 2017 February 22. Available from: <https://doi.org/10.1117/12.2253583>.
24. Roussel C, Dussiot M, Marin M, Morel A, Ndour PA, Duez J, et al. Spherocytic shift of red blood cells during storage provides a quantitative whole cell-based marker of the storage lesion. *Transfusion* 2017;**57**:1007–18.
25. Gérard D, Fattet AJ, Brakta C, Phulpin A, Steschenko D, Lesesve JF, et al. Evaluation of OSMOCELLS, a new semi-automatic device for osmotic fragility assessment. *Int J Lab Hematol* 2017;**39**:521–7.
26. Clark MR, Mohandas N, Shohet SB. Osmotic gradient ektacytometry: comprehensive characterization of red cell volume and surface maintenance. *Blood* 1983;**61**:899–910.
27. Renoux C, Faivre M, Bessaa A, Da Costa L, Joly P, Gauthier A, et al. Impact of surface-area-to-volume ratio, internal viscosity and membrane viscoelasticity on red blood cell deformability measured in isotonic condition. *Sci Rep* 2019;**9**:6771.
28. Lavazec C, Deplaine G, Safeukui I, Perrot S, Milon G, Mercereau-Puijalon O, et al. Microspherulization: a microsphere matrix to explore erythrocyte deformability. *Methods Mol Biol* 2013;**923**:291–7.
29. Dufour E, Gay F, Aguera K, Scoazec JY, Horand F, Lorenzi PL, et al. Pancreatic tumor sensitivity to plasma L-asparagine starvation. *Pancreas* 2012;**41**:940–8.
30. Klei TRL, Meinderts SM, van den Berg TK, van Bruggen R. From the cradle to the grave: the role of macrophages in erythropoiesis and erythrophagocytosis. *Front Immunol* 2017;**8**:73.
31. Sukhbaatar N, Weichhart T. Iron regulation: macrophages in control. *Pharmaceuticals (Basel)* 2018;**11**:137.
32. Garín MI, López RM, Sanz S, Pinilla M, Luque J. Erythrocytes as carriers for recombinant human erythropoietin. *Pharm Res (NY)* 1996;**13**:869–74.
33. Kravtsoff R, Urvoase E, Chambon C, Ropars C. Gd-DOTA loaded into red blood cells, a new magnetic resonance imaging contrast agents for vascular system. *Adv Exp Med Biol* 1992;**326**:347–54.
34. Sayyadipour F, Amirizadeh N, Oodi A, Khalili M, Saba F. Red blood cells are appropriate carrier for coagulation factor VIII. *Cardiovasc Hematol Disord Drug Targets* 2020;**20**:131–7.
35. Leung P, Davis RW, Yao CC, Cannon EP, Way JL. Rhodanese and sodium thiosulfate encapsulated in mouse carrier erythrocytes. II. *In vivo* survivability and alterations in physiologic and morphologic characteristics. *Fundam Appl Toxicol* 1991;**16**:559–66.
36. Gutiérrez Millán C, Bax BE, Castañeda AZ, Marinero MLS, Lanao JM. *In vitro* studies of amikacin-loaded human carrier erythrocytes. *Transl Res* 2008;**152**:59–66.
37. Lamarre Y, Bourgeaux V, Pichon A, Hardeman MR, Campion Y, Hardeman-Zijp M, et al. Effect of inositol hexaphosphate-loaded red blood cells (RBCs) on the rheology of sickle RBCs. *Transfusion* 2013;**53**:627–36.
38. Huisjes R, Bogdanova A, van Solinge WW, Schifflers RM, Kaestner L, van Wijk R. Squeezing for life—properties of red blood cell deformability. *Front Physiol* 2018;**9**:656.
39. Deplaine G, Safeukui I, Jeddi F, Lacoste F, Brousse V, Perrot S, et al. The sensing of poorly deformable red blood cells by the human spleen can be mimicked *in vitro*. *Blood* 2011;**117**:e88–95.
40. Safeukui I, Buffet PA, Perrot S, Sauvanet A, Aussilhou B, Dokmak S, et al. Surface area loss and increased sphericity account for the splenic entrapment of subpopulations of plasmodium falciparum ring-infected erythrocytes. *PLoS One* 2013;**8**:e60150.
41. Safeukui I, Buffet PA, Deplaine G, Perrot S, Brousse V, Sauvanet A, et al. Sensing of red blood cells with decreased membrane deformability by the human spleen. *Blood Adv* 2018;**2**:2581–7.
42. Safeukui I, Buffet PA, Deplaine G, Perrot S, Brousse V, Ndour A, et al. Quantitative assessment of sensing and sequestration of spherocytic erythrocytes by the human spleen. *Blood* 2012;**120**:424–30.
43. Laczko J, Feó CJ, Phillips W. Discocyte—echinocyte reversibility in blood stored in CPD over a period of 56 days. *Transfusion* 1979;**19**:379–88.
44. Svetina S. Red blood cell shape and deformability in the context of the functional evolution of its membrane structure. *Cell Mol Biol Lett* 2012;**17**:171–81.
45. Greenwalt TJ. The how and why of exocytic vesicles. *Transfusion* 2006;**46**:143–52.
46. Harisa GI, Badran MM, Alanazi FK. Erythrocyte nanovesicles: biogenesis, biological roles and therapeutic approach: erythrocyte nanovesicles. *Saudi Pharm J* 2017;**25**:8–17.
47. Almirazq RJ, Seghatchian J, Holovati JL, Acker JP. Extracellular vesicle characteristics in stored red blood cell concentrates are

- influenced by the method of detection. *Transfus Apher Sci* 2017;**56**:254–60.
48. Rubin O, Crettaz D, Canellini G, Tissot JD, Lion N. Microparticles in stored red blood cells: an approach using flow cytometry and proteomic tools. *Vox Sang* 2008;**95**:288–97.
  49. Bardyn M, Rappaz B, Jaferzadeh K, Crettaz D, Tissot JD, Moon I, et al. Red blood cells ageing markers: a multi-parametric analysis. *Blood Transfus* 2017;**15**:239–48.
  50. Almizraq RJ, Holovati JL, Acker JP. Characteristics of extracellular vesicles in red blood concentrates change with storage time and blood manufacturing method. *Transfus Med Hemother* 2018;**45**:185–93.
  51. Lang F, Abed M, Lang E, Föller M. Oxidative stress and suicidal erythrocyte death. *Antioxid Redox Signal* 2013;**21**:138–53.
  52. Reisz JA, Wither MJ, Dzieciatkowska M, Nemkov T, Issaian A, Yoshida T, et al. Oxidative modifications of glyceraldehyde 3-phosphate dehydrogenase regulate metabolic reprogramming of stored red blood cells. *Blood* 2016;**128**:e32–42.
  53. Heaton A, Keegan T, Holme S. *In vivo* regeneration of red cell 2,3-diphosphoglycerate following transfusion of DPG-depleted AS-1, AS-3 and CPDA-1 red cells. *Br J Haematol* 1989;**71**:131–6.
  54. Sparrow RL. Time to revisit red blood cell additive solutions and storage conditions: a role for “omics” analyses. *Blood Transfus* 2012;**10** Suppl 2:s7–11.
  55. Lagerberg JW, Korsten H, van der Meer PF, de Korte D. Prevention of red cell storage lesion: a comparison of five different additive solutions. *Blood Transfus* 2017;**15**:456–62.
  56. D’Alessandro A, Gray AD, Szczepiorkowski ZM, Hansen K, Herschel LH, Dumont LJ. Red blood cell metabolic responses to refrigerated storage, rejuvenation, and frozen storage. *Transfusion* 2017;**57**:1019–30.
  57. Barshtein G, Arbell D, Livshits L, Gural A. Is it possible to reverse the storage-induced lesion of red blood cells?. *Front Physiol* 2018;**9**:914.
  58. Koshkaryev A, Zelig O, Manny N, Yedgar S, Barshtein G. Rejuvenation treatment of stored red blood cells reverses storage-induced adhesion to vascular endothelial cells. *Transfusion* 2009;**49**:2136–43.
  59. Chang AL, Kim Y, Seitz AP, Schuster RM, Pritts TA. pH modulation ameliorates the red blood cell storage lesion in a murine model of transfusion. *J Surg Res* 2017;**212**:54–9.